Key factors in simulating the equatorial Atlantic zonal sea surface temperature gradient in a coupled general circulation model

Tomoki Tozuka,[1] Takeshi Doi,[2] Takafumi Miyasaka,[1] Noel Keenlyside,[3] and Toshio Yamagata[1]

Received 10 October 2010; revised 22 February 2011; accepted 31 March 2011; published 18 June 2011.

[1] Causes of the coupled model bias in simulating the zonal sea surface temperature (SST) gradient in the equatorial Atlantic are examined in three versions of the same coupled general circulation model (CGCM) differing only in the cumulus convection scheme. One version of the CGCM successfully simulates the mean zonal SST gradient of the equatorial Atlantic, in contrast to the failure of the Coupled Model Intercomparison Project phase 3 models. The present analysis shows that key factors to be successful are high skills in simulating the meridional location of the Intertropical Convergence Zone, the precipitation over northern South America, and the southerly winds along the west coast of Africa associated with the West African monsoon in boreal spring. Model biases in the Pacific contribute to the weaker precipitation over northern South America. Uncoupled experiments with the atmospheric component further confirm the importance of remote influences on the development of the equatorial Atlantic bias.

Citation: Tozuka, T., T. Doi, T. Miyasaka, N. Keenlyside, and T. Yamagata (2011), Key factors in simulating the equatorial Atlantic zonal sea surface temperature gradient in a coupled general circulation model, *J. Geophys. Res.*, *116*, C06010, doi:10.1029/2010JC006717.

1. Introduction

[2] Modeling the mean climate state reasonably is the first step toward simulating as well as predicting climate variations. In the equatorial Atlantic, state-of-the-art coupled general circulation models (CGCMs) are not sufficient in this regard: the zonal sea surface temperature (SST) gradient is incorrectly simulated in most CGCMs with model SST cooler in the west than in the east [*Davey et al.*, 2002]. Since the cold tongue is the integral part of the zonal mode or Atlantic Niño, this dominant climate mode in the equatorial Atlantic cannot be simulated or predicted by these CGCMs [*Stockdale et al.*, 2006].

[3] Many studies have been devoted to diagnosing and understanding this model bias. *Biasutti et al.* [2006] examined the Intertropical Convergence Zone (ITCZ) in atmospheric general circulation models (AGCMs) and found that the ITCZ in the Atlantic shifts too far south in boreal spring and leads to excessive precipitation in the Southern Hemisphere. Using outputs from CGCMs, *Richter and Xie* [2008] showed that the westerly wind bias in boreal spring, which also exists in uncoupled AGCMs, deepens the thermocline in the east and hampers the seasonal development of the cold tongue in boreal summer. This zonal wind bias is suggested to be linked with the erroneous zonal precipitation distribution [*Chang et al.*, 2007; *Richter and Xie*, 2008; *Wahl et al.*, 2010]. Also, *Breugem et al.* [2008] pointed out that most Coupled Model Intercomparison Project phase 3 (CMIP3) models simulate a spurious barrier layer in the southeastern tropical Atlantic due to excessive rainfall there. Their results suggest that the barrier layer may significantly contribute to the warm SST bias by suppressing the entrainment of cold water from below [*Hazeleger and Haarsma*, 2005].

[4] Most past studies used models with a variety of parameterization schemes, horizontal resolutions, and oceanic and atmospheric components of CGCM, and thus it was quite difficult to isolate the main causes of the model bias in the equatorial Atlantic. In this regard, *Braconnot et al.* [2007] used outputs from the same CGCM with a single difference in cumulus convection scheme. However, their main focus was on the seasonal march of the ITCZ and the model could not simulate a realistic zonal SST gradient in the equatorial Atlantic.

[5] To further narrow down the causes of the model bias, we analyze three versions of the same CGCM differing only in the cumulus convection scheme. Since one version is quite successful in simulating the zonal SST gradient, the present approach may shed new light on the causes of the equatorial Atlantic bias. This paper is organized as follows. A brief description of the CGCM is given in the next section. In section 3, we compare the zonal SST gradient in the equatorial Atlantic simulated in the CGCM and examine possible causes of their differences. Results from uncoupled AGCM experiments are presented to discuss the remote influence on

[1]Department of Earth and Planetary Science, Graduate School of Science, University of Tokyo, Tokyo, Japan.
[2]NOAA Geophysical Fluid Dynamics Laboratory, Princeton University, Princeton, New Jersey, USA.
[3]Leibniz Institute of Marine Sciences, University of Kiel, Kiel, Germany.

0148-0227/11/2010JC006717

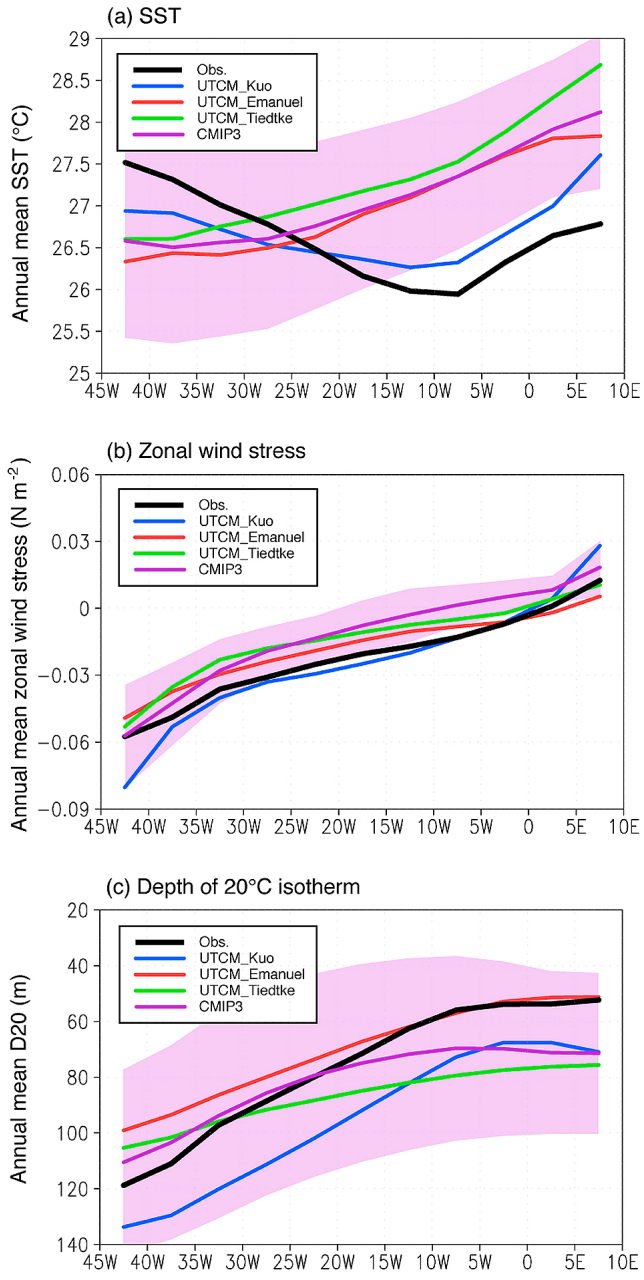

Figure 1. Annual mean (a) sea surface temperature (SST), (b) zonal wind stress, and (c) depth of 20°C isotherm (D20) in the equatorial (2°S–2°N) Atlantic. The shading shows the spread (1 standard deviation) of 22 Coupled Model Intercomparison Project phase 3 (CMIP3) models.

the Atlantic bias in section 4. Conclusions are given in the final section.

2. Model and Data

[6] The CGCM used in this study is the University of Tokyo Coupled general circulation Model (UTCM) [*Tozuka et al.*, 2006]. The atmospheric component was developed at Climate Variations Research Program of Frontier Research System for Global Change of JAMSTEC and is called Frontier Atmospheric General Circulation Model (FrAM) [*Guan et al.*, 2000]. Its T42L28 version is coupled to the oceanic component, Modular Ocean Model version 3.0 (R. C. Pacanowski and S. M. Griffies, MOM 3.0 manual, online report, Princeton Univ., Princeton, N. J., 1999, available at http://www.gfdl.noaa.gov/cms-filesystem-action/model_development/ocean/mom3_manual.pdf), using the UTCM coupler [*Tozuka et al.*, 2006]. Fluxes are exchanged daily and no form of flux adjustments is used. The ocean general circulation model (OGCM) covers the global ocean from 65°S to 65°N, and a monthly climatology [*Levitus and Boyer*, 1994; *Levitus et al.*, 1994] is used poleward of these latitudes. The horizontal resolution varies from 0.4° in the region 92°–140°E, 16°S–30°N to 2° in the outer region [*Tozuka et al.*, 2009]. There are 25 vertical levels with 9 levels in the upper 110 m. The bottom topography adopted in this model is based on 5 min Earth Topography (ETOPO5) data set. No sea ice model is included. For the parameterization of cumulus convection, schemes developed by *Kuo* [1974], *Emanuel* [1991], and *Tiedtke* [1989] are used in this study (see *Stensrud* [2007] for a review). We call these three experiments UTCM_Kuo, UTCM_Emanuel, and UTCM_Tiedtke, respectively. For the land surface model, we used that of *Viterbo and Beljaars* [1995]. The monthly mean climatology from the last 30 years of the total 50 year model integration is used in the present analysis. More details on the CGCM can be found in the work of *Tozuka et al.* [2006] and *Doi et al.* [2010].

[7] To compare with other coupled models, output from the 20c3m (20th Century Climate in Coupled Models) control runs of 22 CGCMs submitted to the World Climate Research Programme's (WCRP's) CMIP3 multimodel data set [*Meehl et al.*, 2007] are used (see *Yokoi et al.* [2009, Table 1] for the list of 22 models). We use the last 50 years to construct monthly climatology. We also use the Hadley Centre Sea Ice and Sea Surface Temperature data set (HadISST) [*Rayner et al.*, 2003] for SST; *World Ocean Atlas 2005* (WOA2005) [*Locarnini et al.*, 2006] for subsurface ocean temperature data; Climate Prediction Center (CPC) Merged Analysis of Precipitation (CMAP) [*Xie and Arkin*, 1996] and Global Precipitation Climatology Project (GPCP) [*Adler et al.*, 2003] for precipitation data; the National Centers for Environmental Prediction (NCEP)–National Center for Atmospheric Research (NCAR) reanalysis data [*Kalnay et al.*, 1996] for wind stress, wind, and sea level pressure (SLP); and *Kubota et al.* [2002] for wind stress data based on QuikSCAT (QSCAT) satellite observation.

3. Simulated Zonal SST Gradient in the Equatorial Atlantic

[8] The observed annual mean SST along the equatorial Atlantic decreases by 1.6°C from 27.5°C at 42.5°W to 25.9°C at 7.5°W (Figure 1a). The sign of SST gradient is surprisingly well simulated by UTCM_Kuo, even if the east-west SST difference is only about one half of that in the observation. This situation is in contrast with the CMIP3 models [*Richter and Xie*, 2008], UTCM_Emanuel, and UTCM_Tiedtke, where the annual mean SST is warmer in the east. The annual mean zonal wind stress is also best simulated by UTCM_Kuo, whereas that in others is weaker than the observed (Figure 1b). It is somewhat surprising that all models simulate

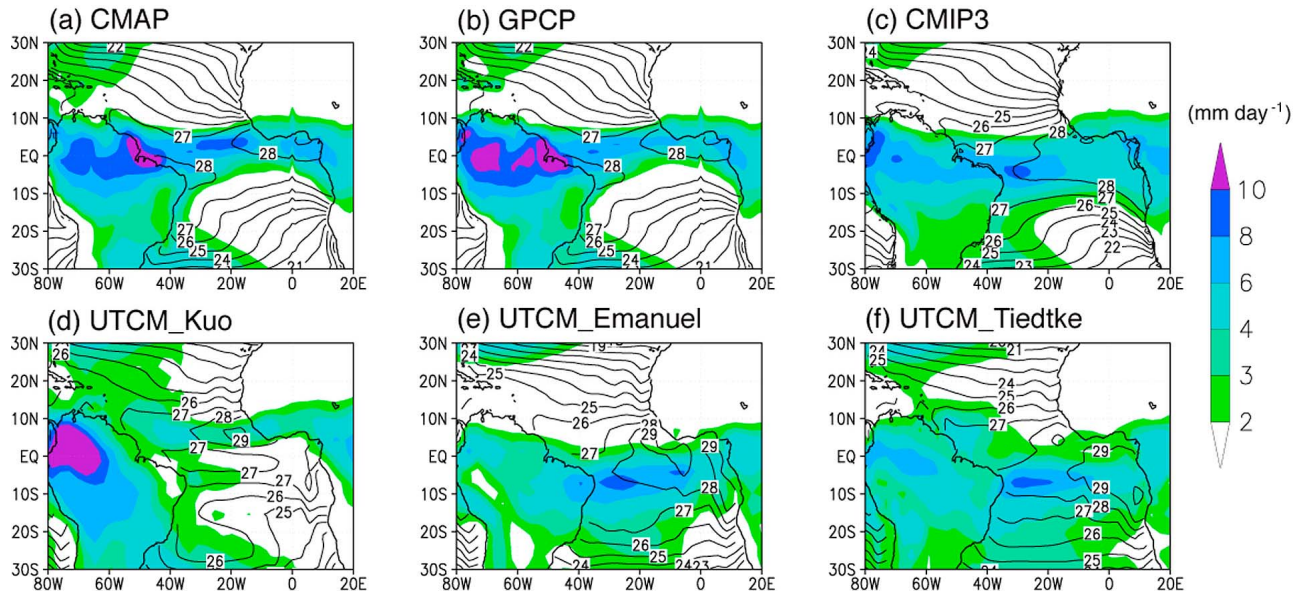

Figure 2. SST (in °C) and precipitation (in mm d^{-1}) in boreal spring (March–May) for (a) Merged Analysis of Precipitation (CMAP)/Hadley Centre Sea Ice and Sea Surface Temperature data set (HadISST), (b) Global Precipitation Climatology Project (GPCP)/HadISST, (c) multimodel mean of CMIP3 coupled general circulation models (CGCMs), (d) University of Tokyo Coupled general circulation Model (UTCM)_Kuo, (e) UTCM_Emanuel, and (f) UTCM_Tiedtke. Contour interval for SST is 1°C, and color shading used for precipitation is shown by the color bar.

the easterly wind stress even though all models except UTCM_Kuo show warmer SST to the east. This contradiction with the well-known result based on the work of *Lindzen and Nigam* [1987] suggests that processes over land or remote forcing may play an important role in the wind pattern of the equatorial Atlantic [*Li and Philander*, 1997]. As a result of the good skill in simulating the easterly trade winds, the zonal difference in the equatorial thermocline depth (depth of 20°C isotherm or D20) between 40°W and 0°E (Figure 1c) is 64 m in UTCM_Kuo, in good agreement with 68 m in the WOA2005. It is much smaller in UTCM_Emanuel, UTCM_Tiedtke, and the 22 CMIP3 multimodel ensemble: 44 m, 28 m, and 38 m, respectively. A stronger tilt in the thermocline leads to a stronger SST gradient through oceanic mixed layer processes. Thus, our model may provide a good means to improve the skill of CGCMs to simulate the mean SST state in the equatorial Atlantic.

[9] Since the cold tongue starts to develop in boreal spring [*Richter and Xie*, 2008], we focus on this key season. Two main features stand out from a comparison of precipitation patterns in boreal spring (March–May; Figure 2). First, a distinct difference is seen over the northern part of the South American continent; large amount of precipitation over 10 mm d^{-1} is found only in the observation and UTCM_Kuo. This favors the easterly trade winds along the equatorial Atlantic as winds converge toward this center of convection. In contrast, the precipitation over northern South America is underestimated in UTCM_Emanuel and UTCM_Tiedtke.

[10] To determine the cause of this model bias, the global precipitation in boreal spring is checked (Figure 3). The Pacific ITCZ is broad and weak in UTCM_Kuo, whereas it is very pronounced in the Southern Hemisphere in UTCM_Emanuel and UTCM_Tiedtke. The broader ITCZ in UTCM_Kuo may be explained by the fact that the Kuo scheme assumes the convective precipitation rate to be proportional to the total-column large-scale moisture convergence. In contrast, the Emanuel scheme does not use this assumption and considers the collective effects of subparcels, and the mass flux at the cloud base is determined by convective available potential energy in the Tiedtke scheme implemented in UTCM [*Nordeng*, 1994].

[11] The precipitation bias in the Pacific in UTCM_Emanuel and UTCM_Tiedtke is closely linked with the SST bias; both have the maximum SST in the Southern Hemisphere across the Pacific (Figure 4). Since the unrealistically strong precipitation in the eastern tropical Pacific along 10°S is relatively close to South America, this bias may have a strong influence on the rainfall over northern South America. To examine this possibility, we have plotted velocity potential and divergent wind at 200 hPa (Figure 5). In the reanalysis data, the strongest divergence in the upper troposphere exists in the western equatorial Pacific, and the convergence occurs in the eastern Pacific. On the other hand, the divergence is centered around 160°W in UTCM_Kuo, 130°W in UTCM_Emanuel, and 120°W in UTCM_Tiedtke. Because the divergent wind emanating from this divergence center reaches South America and converges there in UTCM_Emanuel and UTCM_Tiedtke, it may suppress the convection over northern South America. We note that the velocity potential is weaker in UTCM_Emanuel than in UTCM_Kuo despite that the precipitation is more intense in UTCM_Emanuel, because the ITCZ in UTCM_Emanuel is much narrower.

[12] Another obvious difference of UTCM_Kuo from UTCM_Emanuel, UTCM_Tiedtke, and the ensemble of CMIP3 models is the location of the Atlantic maritime ITCZ in boreal spring; the ITCZ in UTCM_Kuo is located north of

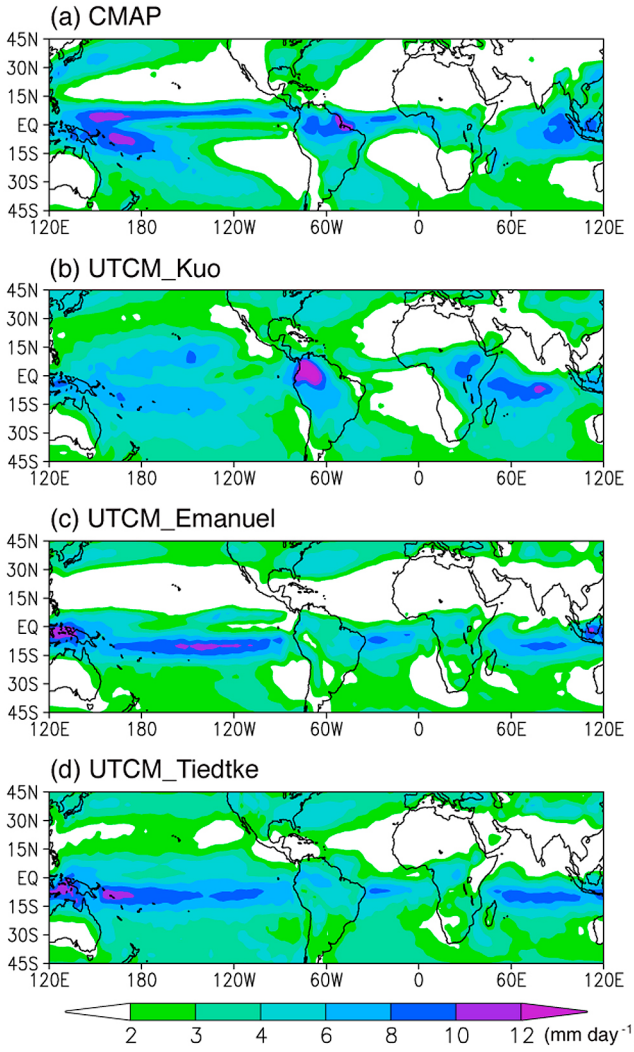

Figure 3. Precipitation (in mm d^{-1}, as shown in the color bar) in boreal spring (March–May) for (a) CMAP, (b) UTCM_Kuo, (c) UTCM_Emanuel, and (d) UTCM_Tiedtke.

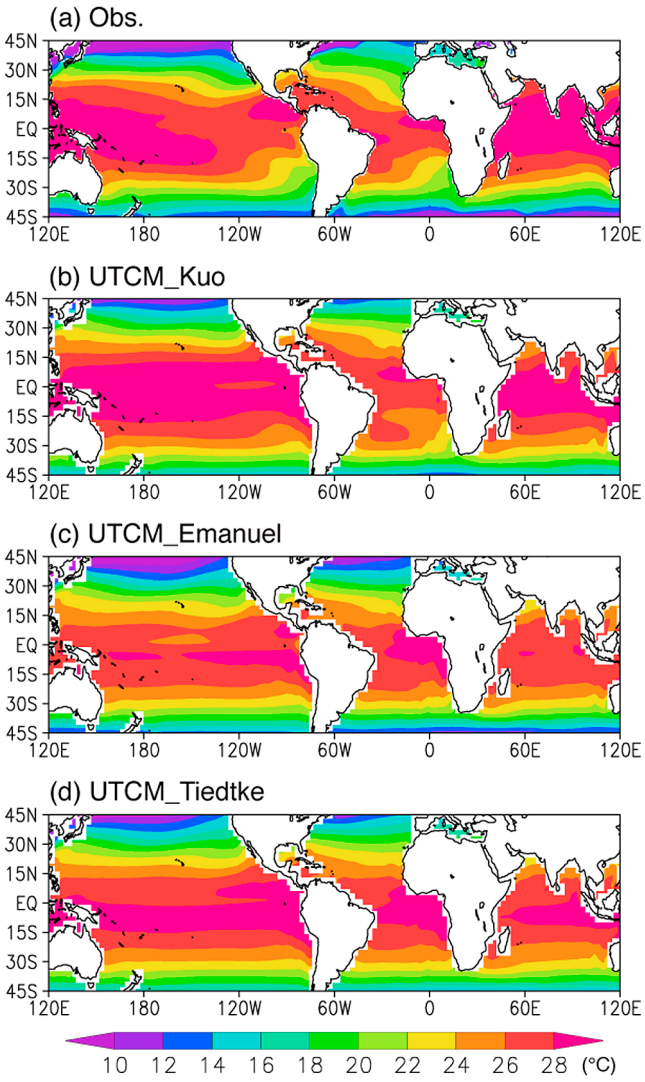

Figure 4. SST (in °C, as shown in the color bar) in boreal spring (March–May) for (a) observation, (b) UTCM_Kuo, (c) UTCM_Emanuel, and (d) UTCM_Tiedtke.

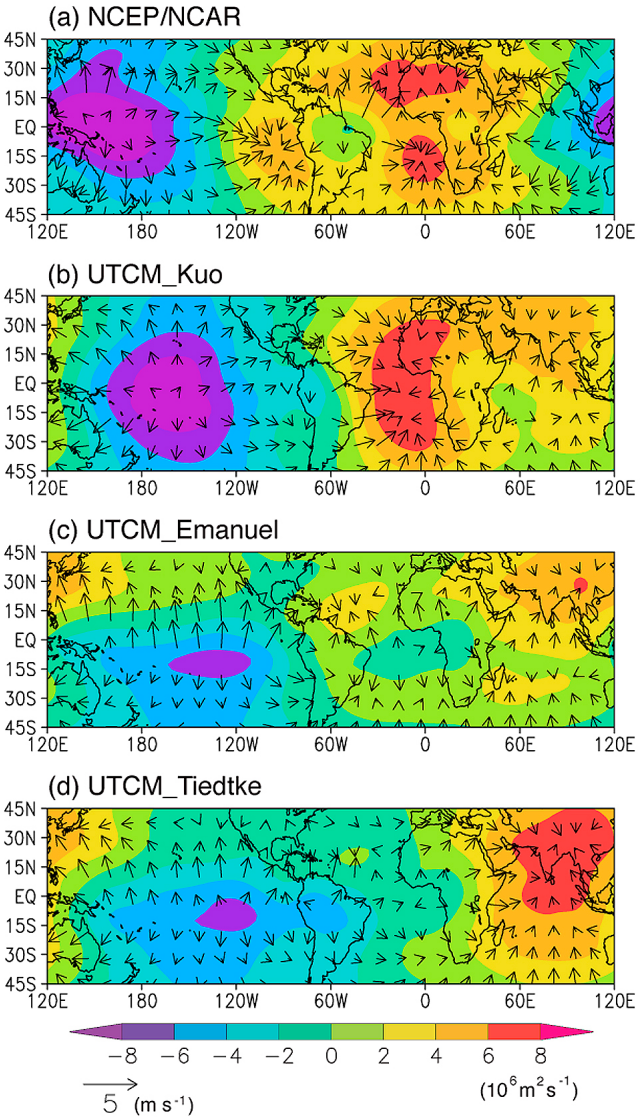

Figure 5. Velocity potential (in $m^2\ s^{-1}$, as shown in the color bar) and divergent wind (in $m\ s^{-1}$ and its magnitude shown in the vector below the color bar) at 200 hPa in boreal spring for (a) National Centers for Environmental Prediction (NCEP)–National Center for Atmospheric Research (NCAR) reanalysis data, (b) UTCM_Kuo, (c) UTCM_Emanuel, and (d) UTCM_Tiedtke.

the equator as observed (Figure 6a) if the location of ITCZ is defined as the latitude at which the meridional wind stress becomes zero. This favors the southeasterly trade winds near the equator in UTCM_Kuo (Figure 6b) and thus the development of the cold tongue [*Richter and Xie*, 2008]. However, several CMIP3 models fail to reproduce the zonal SST gradient even though the meridional location of the ITCZ is in agreement with the observation [*Doi et al.*, 2010]. Therefore, we need to identify other players that may influence the zonal SST gradient.

[13] The alongshore southerly wind stress in the eastern Atlantic induces coastal upwelling along the West African coast in the Southern Hemisphere, which then extends westward by advection and Rossby wave propagation. Thus, the cold SST distributes in the eastern equatorial region [*Philander and Pacanowski*, 1981]. For this reason, we have checked whether this cross-equatorial wind stress plays a role in the better simulation of the cold tongue (Figure 7a). The simulated southerly wind stress in UTCM_Kuo is very close to that in the QSCAT observation and the NCEP-NCAR reanalysis data. In contrast, it is significantly weaker in UTCM_Emanuel, UTCM_Tiedtke, and the ensemble mean of the CMIP3 models. This suggests that the strength of alongshore southerly winds is also responsible for determining the zonal SST gradient. In this context, we note that *Hazeleger and Haarsma* [2005] showed that the coastal upwelling in the southeastern tropical Atlantic reduces the zonal SST bias, by examining entrainment efficiency.

[14] We know that the southerly winds are closely linked with the West African monsoon [*Mitchell and Wallace*, 1992; *Okumura and Xie*, 2004]. As shown in Figure 7b, UTCM_Kuo simulates the meridional SLP difference between the western Sahel region (5°–10°E, 5°–15°N) and the southeastern tropical Atlantic (5°–10°E, 10°S–equator) in boreal spring, in good agreement with the reanalysis data. This supports *Okumura and Xie* [2004], who also suggested that the seasonal development of the cold tongue is closely linked with the intensification of the cross equatorial wind associated with the onset of the West African monsoon.

[15] To check whether the warm SST bias in the southeastern tropical Atlantic expands toward the equator, the

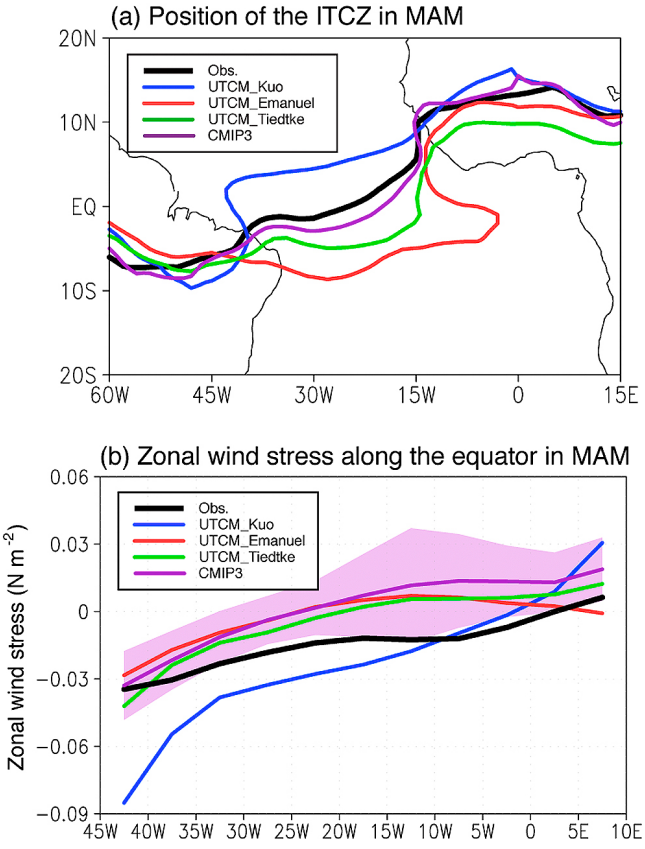

Figure 6. (a) Location of the Intertropical Convergence Zone, defined as a line of zero meridional wind stress, and (b) zonal wind stress along the equatorial Atlantic in boreal spring.

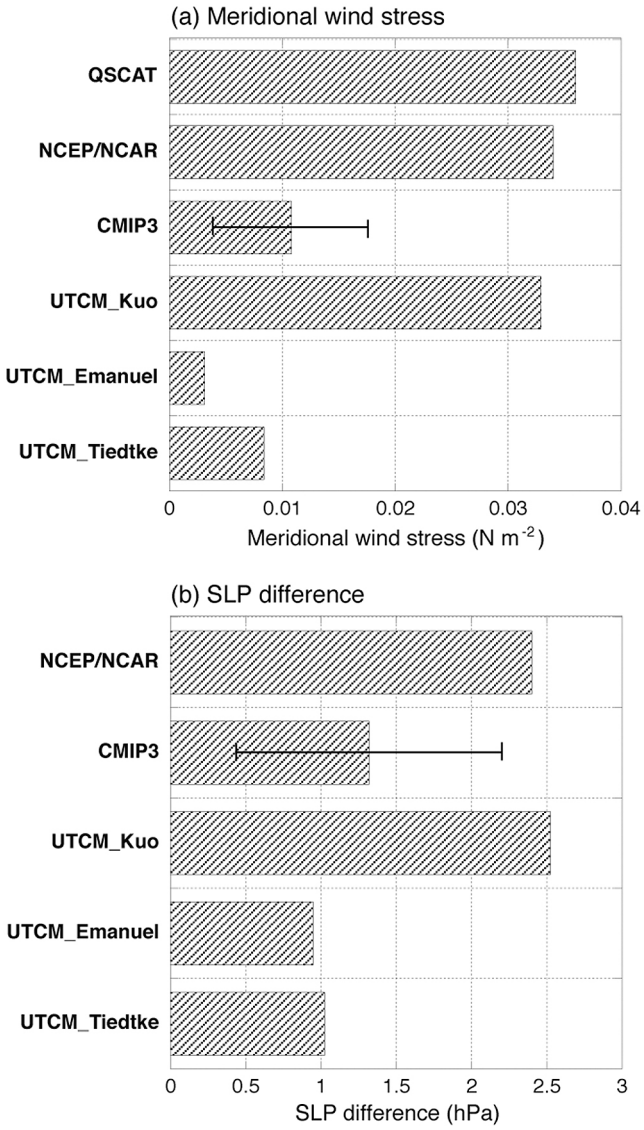

Figure 7. (a) Meridional wind stress in the southeastern tropical Atlantic (5°–10°E, 10°S–equator) in boreal spring (in N m^{-2}). (b) Meridional sea level pressure difference between the western Sahel region (5°–10°E, 5°–15°N) and the southeastern tropical Atlantic (5°–10°E, 10°S–equator) in boreal spring (in hPa). The error bars for the CMIP3 models show their spread (1 standard deviation).

Atlantic SST and wind stress biases in DJF (December–February), MAM (March–May), JJA (June–August), and SON (September–November) are presented in Figure 8. As expected from the weaker southerly wind stress along the West African coast in UTCM_Tiedtke and UTCM_Emanuel in MAM, Figure 8 shows that the warm biases of 5°C or higher exists in the southeastern tropical Atlantic. Then, these warm biases appear to expand equatorward in JJA. These biases may be further amplified by the Bjerknes feedback [*Bjerknes*, 1966]. To see more clearly whether the equatorial bias exists prior to the northward expansion of the warm biases, we have prepared the time-longitude diagram of the SST and wind stress biases along the equatorial Atlantic (Figure 9). Warm SST biases of 1°C or higher exists in UTCM_Emanuel and UTCM_Tiedtke in MAM prior to the equatorward expansion, and this may be due to the equatorial zonal wind biases originating from the biases in the large-scale tropical circulation.

4. AGCM Experiments

[16] To check whether the model biases in other basins may influence the Atlantic bias, we have conducted uncoupled experiments with three versions of FrAM forced with the monthly climatology of the SST data of *Rayner et al.* [2003]. Each version is integrated for 35 years and the last 30 years are used here to construct the climatology. We call these experiments FrAM_Kuo, FrAM_Emanuel, and FrAM_Tiedtke (Table 1).

[17] The ITCZ in the Pacific and the center of the upper level divergence in boreal spring is more realistically simulated in all three AGCM versions (Figures 10 and 11). This may be one reason why the strong precipitation over northern South America (Figure 10), and the easterly wind stress along the equatorial Atlantic (Figure 12a) are reproduced rather well in all three uncoupled experiments.

[18] To examine the effect of the remote forcing, we have conducted three additional experiments (FrAM_Kuo_Atl, FrAM_Emanuel_Atl, and FrAM_Tiedtke_Atl as listed in Table 1). In these experiments, we forced the AGCM with the observed SST in the tropical Atlantic and the SST simulated by UTCM elsewhere. To avoid any jump in the SST at the meridional boundaries (20°S and 20°N), blending regions are inserted such that the observed SST linearly approaches the SST simulated by UTCM poleward of 30°S and 30°N in the Atlantic. Figure 12b shows differences in the zonal wind stress in the equatorial Atlantic between the control and sensitivity experiments in boreal spring. When only the SST over the tropical Atlantic is realistic, the equatorial easterlies become weaker with the Emanuel and Tiedtke schemes. The reduction of the easterlies with the Emanuel and Tiedtke schemes is expected to be amplified by the Bjerknes feedback in the coupled runs [*Bjerknes*, 1966]. These uncoupled experiments support our hypothesis that the biases in the Pacific influence the precipitation over northern South America, and thus the strength of the easterly trade winds in the equatorial Atlantic.

[19] Moreover, a remarkable difference can be found for the precipitation in boreal spring over the tropical Atlantic with the Emanuel scheme (Figure 13). There exists a strong wet bias across the tropical Atlantic south of the equator. This implies that the biases outside of the tropical Atlantic causes the maritime ITCZ in the Atlantic to shift erroneously southward and may explain the most southerly position of the ITCZ among the coupled runs of UTCM with the Emanuel scheme. We also note that the area of precipitation shifts southward over the South American continent for all three schemes.

[20] To further confirm our hypothesis about the remote forcing, we have conducted four additional AGCM experiments (FrAM_Kuo_Atl.E, FrAM_Kuo_Atl.T, FrAM_Emanuel_Atl.K, and FrAM_Tiedtke_Atl.K) as summarized in Table 1. Figure 14 compares the equatorial zonal wind stress among the different experiments in boreal spring. The AGCM with the Emanuel and Tiedtke schemes simulates

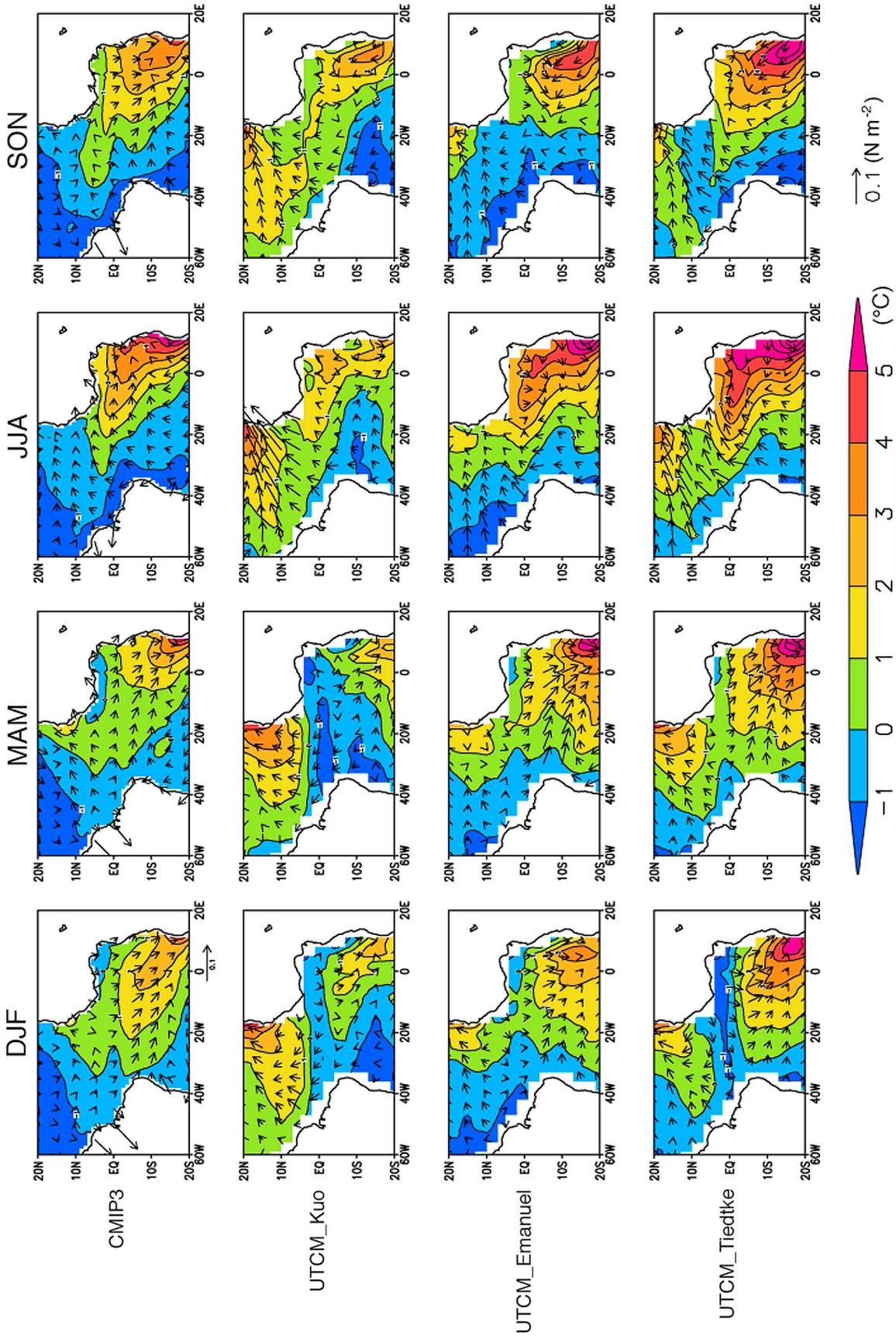

Figure 8. SST (in °C, as shown in the color bar) and wind stress (in N m^{-2} and its magnitude shown in the vector next to the color bar) biases (models minus observation) in DJF, MAM, JJA, and SON.

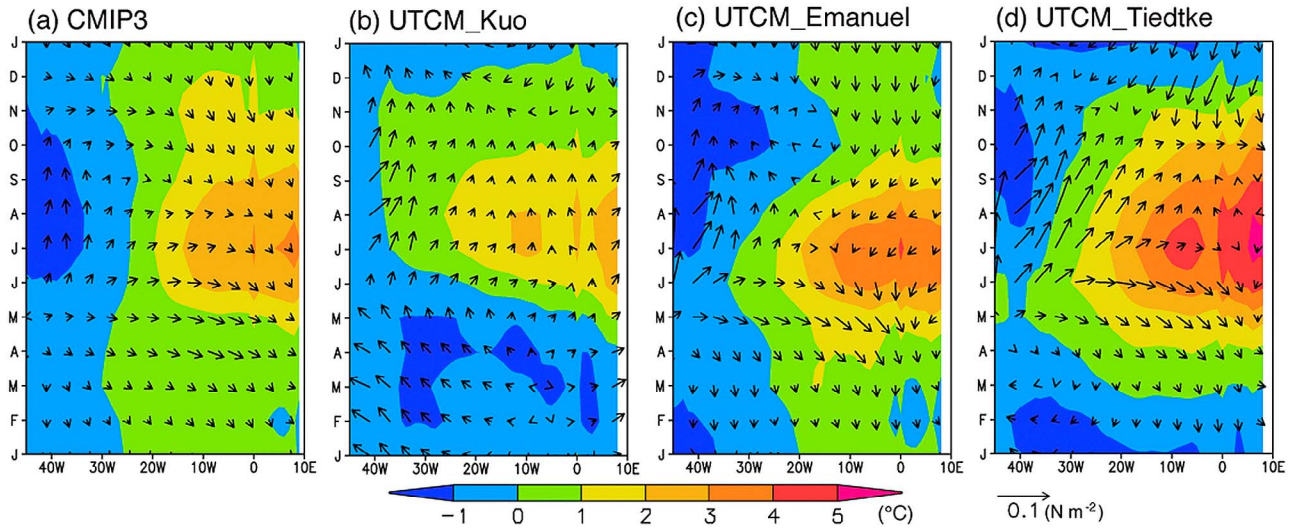

Figure 9. Time-longitude diagrams of SST (in °C, as shown in the color bar) and wind stress (in N m^{-2} and its magnitude shown in the vector next to the color bar) biases (models minus observation) in (a) multimodel mean of CMIP3 CGCMs, (b) UTCM_Kuo, (c) UTCM_Emanuel, and (d) UTCM_Tiedtke.

Table 1. List of AGCM Experiments[a]

Name	Convection Scheme	Tropical Atlantic SST	SST Elsewhere
FrAM_Kuo	Kuo	Observation	Observation
FrAM_Emanuel	Emanuel	Observation	Observation
FrAM_Tiedtke	Tiedtke	Observation	Observation
FrAM_Kuo_Atl	Kuo	Observation	UTCM_Kuo
FrAM_Emanuel_Atl	Emanuel	Observation	UTCM_Emanuel
FrAM_Tiedtke_Atl	Tiedtke	Observation	UTCM_Tiedtke
FrAM_Kuo_Atl.E	Kuo	Observation	UTCM_Emanuel
FrAM_Kuo_Atl.T	Kuo	Observation	UTCM_Tiedtke
FrAM_Emanuel_Atl.K	Emanuel	Observation	UTCM_Kuo
FrAM_Tiedtke_Atl.K	Tiedtke	Observation	UTCM_Kuo

[a]SST, sea surface temperature.

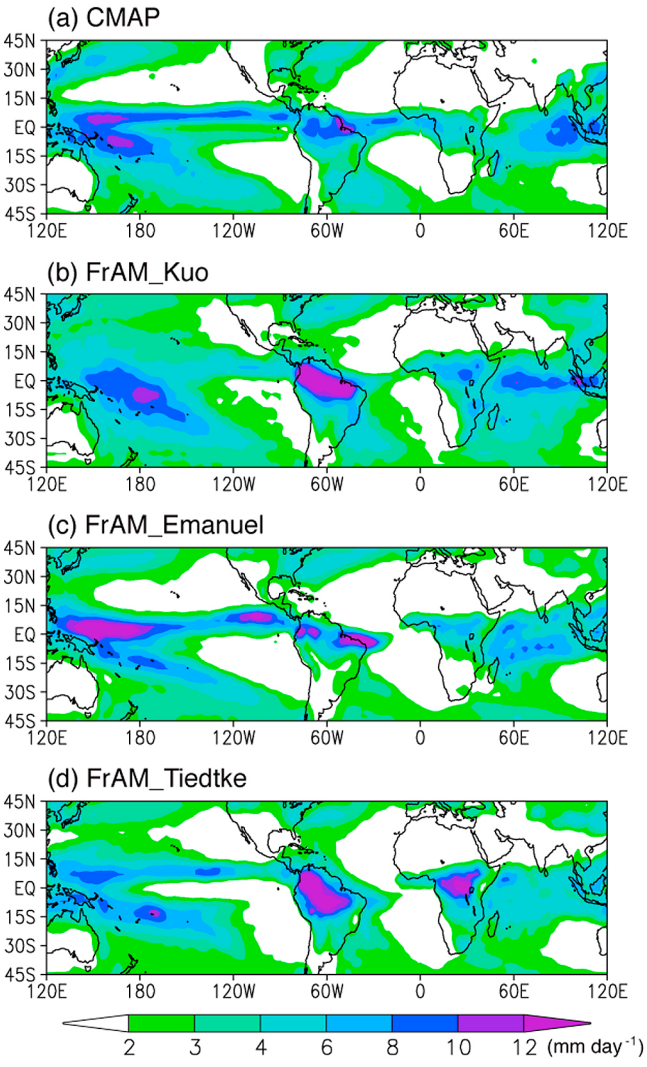

Figure 10. As in Figure 3 but for the atmospheric general circulation model (AGCM) control experiments.

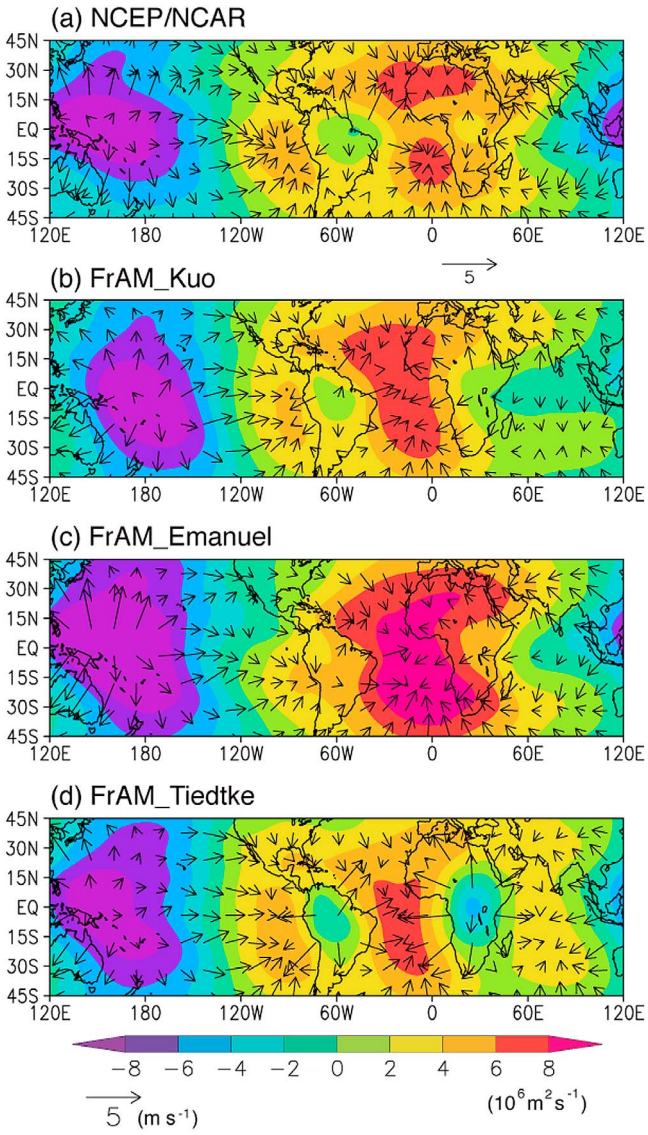

Figure 11. As in Figure 5 but for the AGCM control experiments.

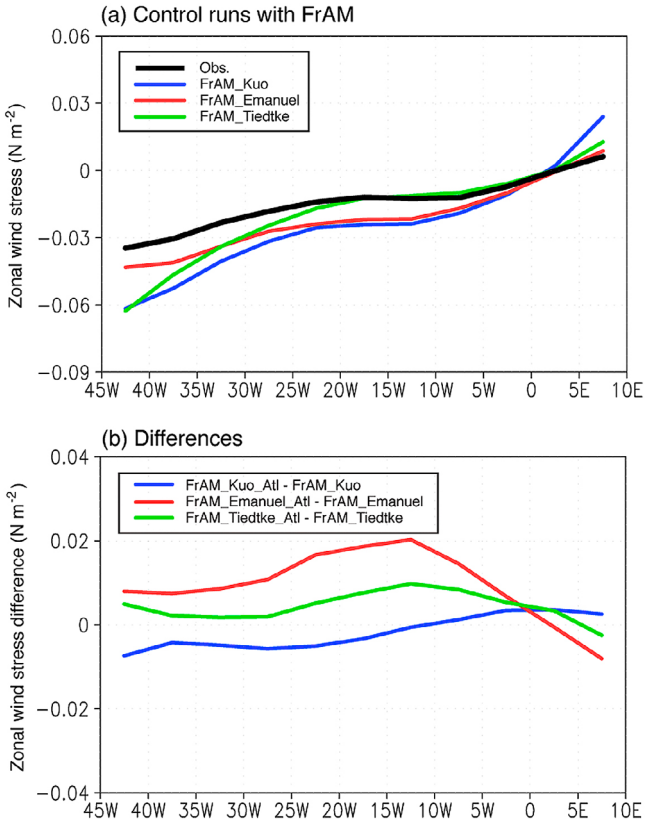

Figure 12. (a) Zonal wind stress in the equatorial (2°S–2°N) Atlantic between the control experiments (FrAM_Kuo, FrAM_Emanuel, and FrAM_Tiedtke) in boreal spring. (b) Differences in the zonal wind stress in the equatorial (2°S–2°N) Atlantic between the control experiments (FrAM_Kuo, FrAM_Emanuel, and FrAM_Tiedtke) and the sensitivity experiments (FrAM_Kuo_Atl, FrAM_Emanuel_Atl, and FrAM_Tiedtke_Atl) in boreal spring.

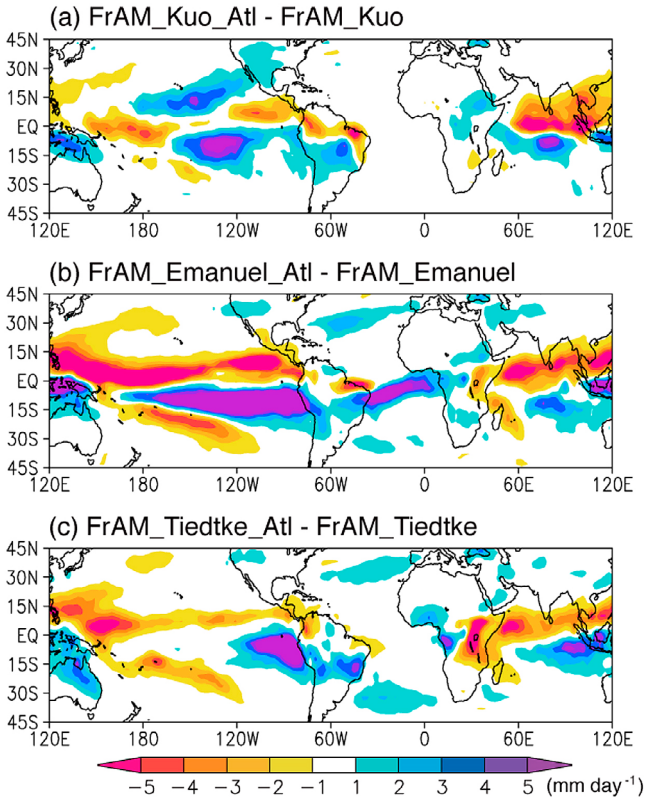

Figure 13. Difference in the precipitation (in mm d^{-1}, as shown in the color bar) in boreal spring (March–May) between the control experiments (FrAM_Kuo, FrAM_Emanuel, and FrAM_Tiedtke) and the sensitivity experiments (FrAM_Kuo_Atl, FrAM_Emanuel_Atl, and FrAM_Tiedtke_Atl).

stronger easterly wind stress over the equatorial Atlantic, when forced by the SST simulated by UTCM_Kuo in the outer regions. On the other hand, the equatorial easterly wind becomes weaker in the AGCM with the Kuo scheme, when the SST simulated by UTCM_Emanuel and UTCM_Tiedtke is used outside of the tropical Atlantic. Therefore, the model biases in the tropical Pacific contribute to the Atlantic bias.

[21] Finally, we address an interesting problem that the changes in the large-scale circulation between the coupled and uncoupled runs are larger with the Emanuel and Tiedtke schemes than with the Kuo scheme. To mediate this difference, we have plotted differences in the skin temperature between the coupled and uncoupled experiments (Figure 15). All three versions of UTCM show warm biases of a similar magnitude in the southeastern Pacific, but cold biases in the western Pacific are much stronger in UTCM_Emanuel and UTCM_Tiedtke than in UTCM_Kuo. As a result, the equatorial zonal SST gradient in the tropical Pacific is smaller than the observation in all three versions. In particular, UTCM_Emanuel and UTCM_Tiedtke show smaller SST gradient than UTCM_Kuo. Thus, the convection center shifts more eastward for the former two cases in the coupled runs (Figure 5) compared with the uncoupled runs (Figure 11).

These changes in the SST gradient lead to changes in the large-scale circulation and precipitation [e.g., *Xie et al.*, 2010]. For instance, the above situation in the Pacific is analogous to an El Niño condition, where the anomalous Walker circulation shows ascent over the eastern Pacific and

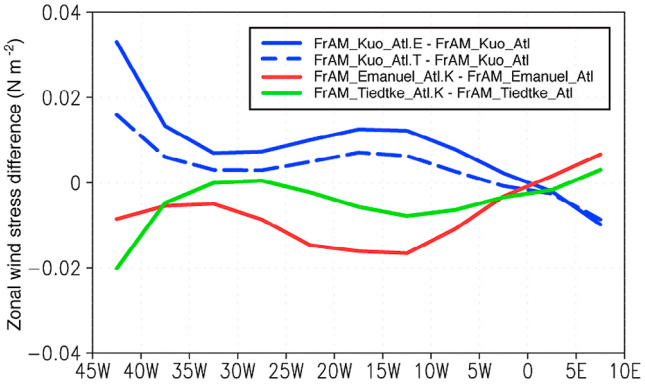

Figure 14. Difference in the annual mean zonal wind stress in the equatorial (2°S–2°N) Atlantic between FrAM_Kuo_Atl.E and FrAM_Kuo_Atl (blue solid line), FrAM_Kuo_Atl.T and FrAM_Kuo_Atl (blue dashed line), FrAM_Emanuel_Atl.K and FrAM_Emanuel_Atl (red solid line), and FrAM_Tiedtke_Atl.K and FrAM_Tiedtke_Atl (green solid line).

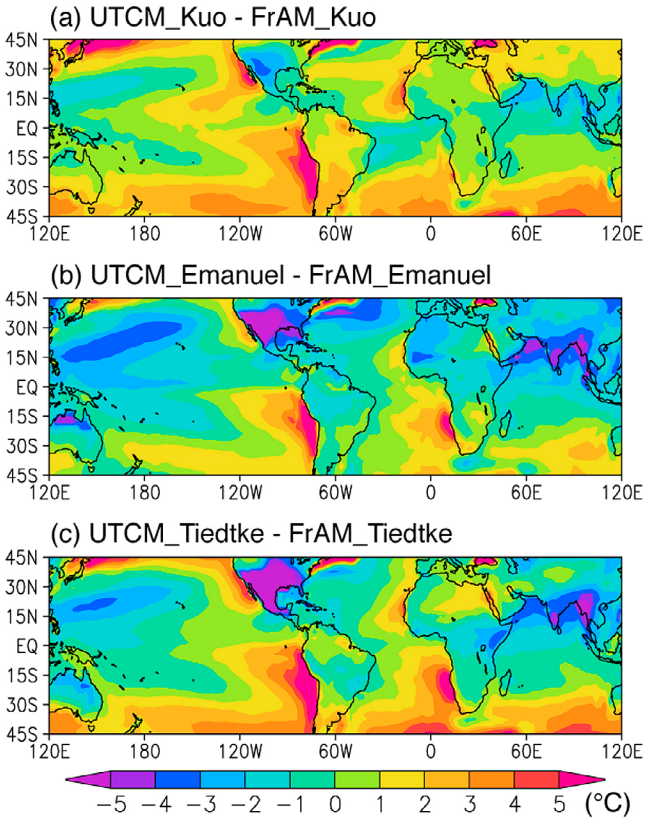

Figure 15. Difference in the skin temperature (in °C) in boreal spring between (a) UTCM_Kuo and FrAM_Kuo, (b) UTCM_Emanuel and FrAM_Emanuel, and (c) UTCM_Tiedtke and FrAM_Tiedtke. For the SST, observed SST is used for FrAM.

descent over the Atlantic [*Wang*, 2005]. In addition, the cooler (warmer) land surface temperature over northern South America in UTCM_Emanuel (UTCM_Kuo) compared with FrAM_Emanuel (FrAM_Kuo) favors weaker (stronger) easterlies in the equatorial Atlantic.

5. Conclusions

[22] We have examined causes of the serious model bias in the zonal SST gradient in the equatorial Atlantic by comparing the performance of three versions of the same CGCM, differing only in the cumulus convection scheme and the CMIP3 models with observations. In contrast to all sophisticated CMIP3 models, one version of our coupled model that implements the cumulus convection scheme of *Kuo* [1974] successfully simulates the mean zonal SST gradient. Thus, we have tried to identify possible causes for this model bias and suggest possible remedies for it, despite that it may be model dependent. It is found that UTCM_Kuo shows high skills in simulating the meridional location of the ITCZ, the precipitation over northern South America continent, and the southerly winds along the west coast of Africa associated with the West African monsoon in boreal spring. All of these are important for simulating the realistic zonal SST gradient. Analysis of the large-scale atmospheric circulation indicates that remote forcing from the Pacific may contribute to the model bias of the precipitation over northern South America.

[23] The cumulus convection scheme of *Kuo* [1974] has been long criticized since observed deep convection is not always controlled by large-scale water supply [*Emanuel and Raymond*, 1993]. Our intention in this study is not to discuss superiority of a particular scheme. In fact, one of the CMIP3 model (i.e., CNRM-CM3) uses the Kuo-type closure for deep convection scheme, but the ITCZ in the tropical Atlantic shifts to the south of the equator and the precipitation over northern South America is underestimated during boreal spring (figure not shown). As a result, the annual mean SST in the equatorial Atlantic is warmer in the east. Thus, the present work with UTCM should be considered as sensitivity experiments of a single coupled model that only differs in the choice of convection scheme. However, our study shows that coupled ocean-atmosphere feedbacks in regions of deep convection is one of the major sources of model error. It may provide a new insight to reconsider even the classic problem of the organized cumulus convection from a viewpoint of ocean-atmosphere coupling. We hope that the present analysis will shed new light on improvement of coupled model performance for both simulation and prediction of the equatorial Atlantic climate.

[24] **Acknowledgments.** Constructive comments provided by two anonymous reviewers helped us to improve the earlier manuscript. We thank Arun Chakraborty and Milind Mujumdar for their contributions during the early stage of development for UTCM. The CGCM was run on HITACHI SR11000/J1 of the Information Technology Center, University of Tokyo, under cooperative research with the Atmosphere and Ocean Research Institute, University of Tokyo. We acknowledge the modeling groups, the Program for Climate Model Diagnosis and Intercomparison (PCMDI), and the WCRP's Working Group on Coupled Modeling (WGCM) for their roles in making available the WCRP CMIP3 multimodel data set. Support of this data set is provided by the Office of Science, U.S. Department of Energy. The present research is supported by JST/JICA through the Science and Technology Research Partnership for Sustainable Development (SATREPS) and by the Japan Society for Promotion of Science through Grant-in-Aid for Young Scientists (B) 21740341 and Grant-in-Aid for Scientific Research (B) 20340125.

References

Adler, R. F., et al. (2003), The Version 2 Global Precipitation Climatology Project (GPCP) monthly precipitation analysis (1979–present), *J. Hydrometeorol.*, *4*, 1147–1167, doi:10.1175/1525-7541(2003)004<1147:TVGPCP>2.0.CO;2.

Biasutti, M., A. H. Sobel, and Y. Kushnir (2006), AGCM precipitation biases in the tropical Atlantic, *J. Clim.*, *19*, 935–958, doi:10.1175/JCLI3673.1.

Bjerknes, J. (1966), A possible response of the atmospheric Hadley circulation to equatorial anomalies of ocean temperature, *Tellus*, *18*, 820–829, doi:10.1111/j.2153-3490.1966.tb00303.x.

Braconnot, P., F. Hourdin, S. Bony, J. L. Dufresne, J. Y. Grandpeix, and O. Marti (2007), Impact of different convective cloud schemes on the simulation of the tropical seasonal cycle in a coupled ocean-atmosphere model, *Clim. Dyn.*, *29*, 501–520, doi:10.1007/s00382-007-0244-y.

Breugem, W.-P., P. Chang, C. J. Jang, J. Mignot, and W. Hazeleger (2008), Barrier layers and tropical Atlantic SST biases in coupled GCMs, *Tellus Ser. A*, *60*, 885–897.

Chang, C.-Y., J. A. Carton, S. A. Grodsky, and S. Nigam (2007), Seasonal climate of the tropical Atlantic sector in the NCAR Community Climate System Model 3: Error structure and probable causes of errors, *J. Clim.*, *20*, 1053–1070, doi:10.1175/JCLI4047.1.

Davey, M. K., et al. (2002), STOIC: A study of coupled model climatology and variability in tropical ocean regions, *Clim. Dyn.*, *18*, 403–420, doi:10.1007/s00382-001-0188-6.

Doi, T., T. Tozuka, and T. Yamagata (2010), The Atlantic Meridional Mode and its coupled variability with the Guinea Dome, *J. Clim.*, *23*, 455–475, doi:10.1175/2009JCLI3198.1.

Emanuel, K. (1991), A scheme for representing cumulus convection in large-scale models, *J. Atmos. Sci.*, *48*, 2313–2329, doi:10.1175/1520-0469(1991)048<2313:ASFRCC>2.0.CO;2.

Emanuel, K. A., and D. J. Raymond (1993), *The Representation of Cumulus Convection in Numerical Models*, *Meteorol. Monogr. Ser.*, vol. 46, 246 pp., Am. Meteorol. Soc., Boston.

Guan, Z., S. Iizuka, M. Chiba, S. Yamane, K. Ashok, M. Honda, and T. Yamagata (2000), Frontier Atmospheric General Circulation Model Version 1.0 (FrAM1.0), model climatology, *Tech. Rep. FTR-1*, 27 pp., Front. Res. Cent. for Global Change, Tokyo.

Hazeleger, W., and R. J. Haarsma (2005), Sensitivity of tropical Atlantic climate to mixing in a coupled ocean-atmosphere model, *Clim. Dyn.*, *25*, 387–399, doi:10.1007/s00382-005-0047-y.

Kalnay, E., et al. (1996), The NCEP/NCAR 40-Year Reanalysis Project, *Bull. Am. Meteorol. Soc.*, *77*, 437–471, doi:10.1175/1520-0477(1996)077<0437:TNYRP>2.0.CO;2.

Kubota, M., N. Iwasaka, S. Kizu, M. Konda, and K. Kutsuwada (2002), Japanese ocean flux data sets with use of remote sensing observations (J-OFURO), *J. Oceanogr.*, *58*, 213–225, doi:10.1023/A:1015845321836.

Kuo, H. L. (1974), Further studies of the parameterization of the influence of cumulus convection on large-scale flow, *J. Atmos. Sci.*, *31*, 1232–1240, doi:10.1175/1520-0469(1974)031<1232:FSOTPO>2.0.CO;2.

Levitus, S., and T. P. Boyer (1994), *World Ocean Atlas 1994*, vol. 4, *Temperature, NOAA Atlas NESDIS*, vol. 4, 129 pp., NOAA, Silver Spring, Md.

Levitus, S., R. Burgett, and T. P. Boyer (1994), *World Ocean Atlas 1994*, vol. 3, *Salinity, NOAA Atlas NESDIS*, vol. 3, 111 pp., NOAA, Silver Spring, Md.

Li, T., and S. G. H. Philander (1997), On the seasonal cycle of the equatorial Atlantic Ocean, *J. Clim.*, *10*, 813–817, doi:10.1175/1520-0442(1997)010<0813:OTSCOT>2.0.CO;2.

Lindzen, R. S., and S. Nigam (1987), On the role of sea surface temperature gradients in forcing low-level winds and convergence in the tropics, *J. Atmos. Sci.*, *44*, 2418–2436, doi:10.1175/1520-0469(1987)044<2418:OTROSS>2.0.CO;2.

Locarnini, R. A., A. V. Mishonov, J. I. Antonov, T. P. Boyer, and H. E. Garcia (2006), *World Ocean Atlas 2005*, vo1. 1, *Temperature, NOAA Atlas NESDIS*, vol. 61, edited by S. Levitus, 182 pp., NOAA, Silver Spring, Md.

Meehl, G. A., C. Covey, T. Delworth, M. Latif, B. McAvaney, J. F. B. Mitchell, K. J. Stouffer, and K. E. Taylor (2007), The WCRP CMIP3 multimodel dataset: A new era in climate change research, *Bull. Am. Meteorol. Soc.*, *88*, 1383–1394, doi:10.1175/BAMS-88-9-1383.

Mitchell, T., and J. M. Wallace (1992), The annual cycle in equatorial convection and sea surface temperature, *J. Clim.*, *5*, 1140–1156, doi:10.1175/1520-0442(1992)005<1140:TACIEC>2.0.CO;2.

Nordeng, T. E. (1994), Extended versions of the convective parameterization scheme at ECMWF and their impact on the mean and transient activity of the model in the tropics, *Tech. Memo.* 206, 41 pp., Eur. Cent. for Medium-Range Weather Forecasts, Reading, U. K.

Okumura, Y., and S.-P. Xie (2004), Interaction of the Atlantic equatorial cold tongue and the African monsoon, *J. Clim.*, *17*, 3589–3602, doi:10.1175/1520-0442(2004)017<3589:IOTAEC>2.0.CO;2.

Philander, S. G. H., and R. C. Pacanowski (1981), The oceanic response to cross-equatorial winds (with application to coastal upwelling in low latitudes), *Tellus*, *33*, 201–210, doi:10.1111/j.2153-3490.1981.tb01744.x.

Rayner, N. A., D. E. Parker, E. B. Horton, C. K. Folland, L. V. Alexander, D. P. Rowell, E. C. Kent, and A. Kaplan (2003), Global analysis of SST, sea ice and night marine air temperature since the late nineteenth century, *J. Geophys. Res.*, *108*(D14), 4407, doi:10.1029/2002JD002670.

Richter, I., and S.-P. Xie (2008), On the origin of equatorial Atlantic biases in coupled general circulation models, *Clim. Dyn.*, *31*, 587–598, doi:10.1007/s00382-008-0364-z.

Stensrud, D. J. (2007), *Parameterization Schemes: Keys to Understanding Numerical Weather Prediction Models*, 459 pp., Cambridge Univ. Press, New York.

Stockdale, T. N., M. A. Balmaseda, and A. Vidard (2006), Tropical Atlantic SST prediction with coupled ocean-atmosphere GCMs, *J. Clim.*, *19*, 6047–6061, doi:10.1175/JCLI3947.1.

Tiedtke, M. (1989), A comprehensive mass flux scheme for cumulus parameterization in large-scale models, *Mon. Weather Rev.*, *117*, 1779–1800, doi:10.1175/1520-0493(1989)117<1779:ACMFSF>2.0.CO;2.

Tozuka, T., T. Miyasaka, A. Chakraborty, M. Mujumdar, S. K. Behera, Y. Masumoto, H. Nakamura, and T. Yamagata (2006), Univ. of Tokyo coupled general circulation model (UTCM1.0), *Ocean Atmos. Res. Rep. 7*, 44 pp., Univ. of Tokyo, Tokyo.

Tozuka, T., T. Qu, Y. Masumoto, and T. Yamagata (2009), Impacts of the South China Sea Throughflow on seasonal and interannual variations the Indonesian Throughflow, *Dyn. Atmos. Oceans*, *47*, 73–85, doi:10.1016/j.dynatmoce.2008.09.001.

Viterbo, P., and A. C. M. Beljaars (1995), An improved land surface parameterization scheme in the ECMWF model and its validation, *J. Clim.*, *8*, 2716–2748, doi:10.1175/1520-0442(1995)008<2716:AILSPS>2.0.CO;2.

Wahl, S., M. Latif, W. Park, and N. Keenlyside (2010), On the tropical Atlantic SST warm bias in the Kiel climate model, *Clim. Dyn.*, *36*, 891–906, doi:10.1007/s00382-009-0690-9.

Wang, C. (2005), ENSO, Atlantic climate variability, and the Walker and Hadley Circulations, in *The Hadley Circulation: Present, Past and Future*, edited by F. Diaz and R. S. Bradley, pp. 173–202, Kluwer Acad., Dordrecht, Netherlands.

Xie, P. P., and P. A. Arkin (1996), Analyses of global monthly precipitation using gauge observations, satellite estimates, and numerical model predictions, *J. Clim.*, *9*, 840–858, doi:10.1175/1520-0442(1996)009<0840:AOGMPU>2.0.CO;2.

Xie, S.-P., C. Deser, G. A. Vecchi, J. Ma, H. Teng, and A. T. Wittenberg (2010), Global warming pattern formation: Sea surface temperature and rainfall, *J. Clim.*, *23*, 966–986, doi:10.1175/2009JCLI3329.1.

Yokoi, T., T. Tozuka, and T. Yamagata (2009), Seasonal variations of the Seychelles Dome simulated in the CMIP3 models, *J. Phys. Oceanogr.*, *39*, 449–457, doi:10.1175/2008JPO3914.1.

T. Doi, NOAA Geophysical Fluid Dynamics Laboratory, Princeton University, Princeton University Forrestal Campus, 201 Forrestal Rd., Princeton, NJ 08540-6649, USA.

N. Keenlyside, Leibniz Institute of Marine Sciences, University of Kiel, Duesternbrooker Weg 20, D-24105 Kiel, Germany.

T. Miyasaka, T. Tozuka, and T. Yamagata, Department of Earth and Planetary Science, Graduate School of Science, University of Tokyo, 7-3-1 Hongo, Bunkyo-ku, Tokyo 113-0033, Japan. (tozuka@eps.s.u-tokyo.ac.jp)